Supporting Info: Electron Transfer and Solvent Mediated Electronic Localization in Molecular Photocatalysis

Asmus O. Dohn,*,† Kasper S. Kjær,‡ Tobias B. Harlang,‡ Sophie E. Canton,¶ Martin M. Nielsen,‡ and Klaus B. Møller†

†*Department of Chemistry, Technical University of Denmark, Kemitorvet 206, 2800 Kgs Lyngby, Denmark*

‡*Department of Physics, Technical University of Denmark, Building 307 2800 Kgs. Lyngby, Denmark*

¶*Center for Ultrafast Imaging, University of Hamburg, 22761 Hamburg, Germany*

E-mail: asod@kemi.dtu.dk

Further Computational Details

The Born-Oppenheimer QM/MM MD simulations were carried out in our own implementation of an additive QM/MM Scheme,[1–3] where the QM and MM regions are interfaced through the total energy of the system:

$$E_{\text{tot}} = E_{\text{QM}} + E_{\text{MM}} + E_{\text{QM/MM}} \tag{1}$$

where the three terms represent the energy of the QM subsystem, the MM subsystem and their interaction energy, respectively. The interaction energy consists of a Coulomb term

between the electronic density and the classical point charges, a Coulomb term between the nuclei in the QM subsystem and the MM point charges, and a Lennard-Jones (LJ) term:

$$E_{\mathrm{QM/MM}} = \sum_{i}^{N_{\mathrm{MM}}} q_i \int \frac{n(\mathbf{r})}{|\mathbf{r} - \mathbf{R}_i|} d\mathbf{r} + \sum_{i}^{N_{\mathrm{MM}}} \sum_{\alpha}^{N_{\mathrm{QM}}} \frac{q_i Z_\alpha}{|\mathbf{R}_\alpha - \mathbf{R}_i|} + E_{\mathrm{LJ}} \tag{2}$$

$$E_{\mathrm{LJ}} = \sum_{i}^{N_{\mathrm{MM}}} \sum_{\alpha}^{N_{\mathrm{QM}}} 4\epsilon_{i\alpha} \left[\left(\frac{\sigma_{i\alpha}}{|\mathbf{R}_\alpha - \mathbf{R}_i|} \right)^{12} - \left(\frac{\sigma_{i\alpha}}{|\mathbf{R}_\alpha - \mathbf{R}_i|} \right)^{6} \right] \tag{3}$$

The LJ parameters are combined using the Waldman-Hagler combination rules.[4]

The first term in eqn. 1 is evaluated with density functional theory (DFT), using the grid-based projector augmented wave method, implemented in the GPAW package,[5] which is modified so that the total effective potential also contains a term from the MM subsystem. The calculations were performed with a localised atomic orbital basis in combination with the real space grid, allowing for high parallelisation as well as fast diagonalization of the principal matrices.

Preliminary Tests and Geometry Relaxations

Basis Sets & Grid Spacing

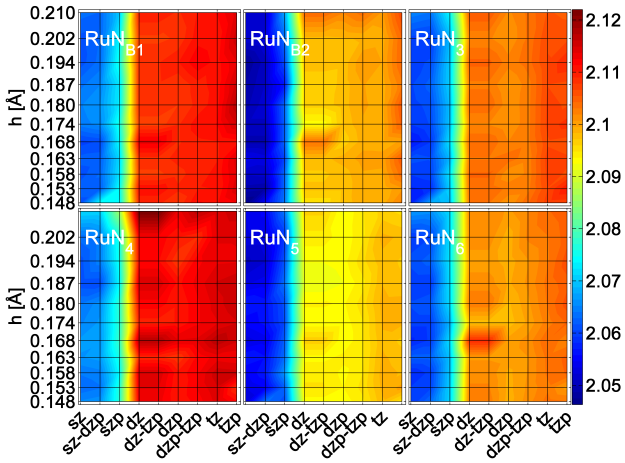

Figure S1: Convergence of the Ru-N distances as a function of grid spacing h and basis set size. The color bar shows the distance in Å.

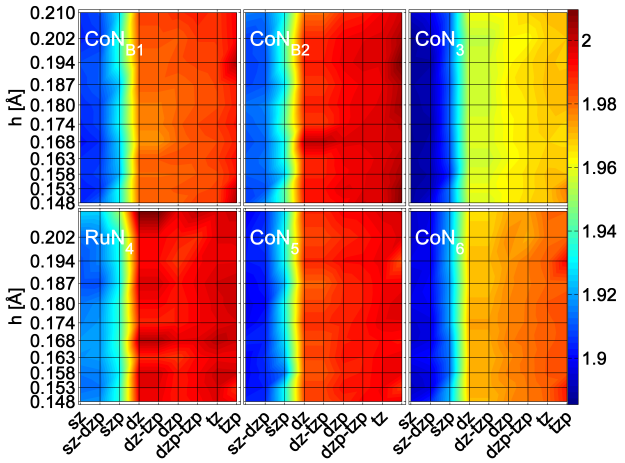

Figure S2: Convergence of the Co-N distances as a function of h and basis set size. The color bar shows the distance in Å.

For the Ru=Co simulations, the QM real space cell size was chosen such that the molecule had 5 Å of extra grid points in each dimension, to avoid truncation of the wave functions, leading to a 25x20x30 Å cell.

Figures S1 and S2 show the convergence of the GS Ru/Co-N distances with respect to grid

spacing and basis set size. In both cases, the major influence on the structure arises from the choice of basis set, which converges rapidly when basis sets of size larger than double zeta are chosen. For all values of 0.15 Å $< h <$ 0.20 Å, the variation in bond distance is at least 17 times smaller than the changes arising from changing the basis, meaning that all grid spacings under 0.20 Å will be acceptable.

Geometry Relaxations

Table S1: Average bond lengths from the QM/MM MD simulations, compared to geometry optimizations using a more conventional quantum chemistry package, ORCA.[6]

	Ru							Co						
Bond:	b_1	b_2	v_1	v_2	d_1	d_2	avg.	b_1	b_2	v_1	v_2	d_1	d_2	avg.
Method	GS													
Orca, PBE, TZVP vacuum	2.110	2.110	2.108	2.109	2.104	2.104	2.108	1.997	1.997	1.968	1.968	1.997	1.976	1.984
Orca, PBE, TZVP COSMO(acn)	2.099	2.099	2.095	2.094	2.091	2.091	2.095	1.965	1.965	1.954	1.955	1.952	1.951	1.957
GPAW QM/MM MD avg.	2.145	2.149	2.145	2.142	2.140	2.139	2.143	2.012	2.012	2.005	2.003	2.001	1.999	2.005
	LS													
Orca, PBE, TZVP vacuum	2.128	2.128	2.111	2.110	2.103	2.102	2.114	2.175	2.173	1.953	1.953	2.067	2.065	2.064
Orca, PBE, TZVP COSMO(acn)	2.109	2.108	2.098	2.099	2.093	2.093	2.100	2.133	2.135	1.942	1.942	2.053	2.053	2.043
Orca, PBE0/6-31G(d,p)*, COSMO(acn)	2.102	2.102	2.087	2.088	2.082	2.081	2.090	1.994	2.206	1.964	1.971	1.972	2.164	2.045
Orca, PBE0/def2-TZVP*, COSMO(acn)	2.097	2.093	2.078	2.083	2.074	2.073	2.083	2.109	2.179	1.974	1.976	2.069	2.126	2.072
Orca, B3LYP/6-31G(d,p)*, COSMO(acn)	2.126	2.129	2.121	2.120	2.110	2.120	2.121	2.124	2.147	1.950	1.952	2.046	2.050	2.045
Orca, B3LYP/def2-TZVP*, COSMO(acn),	2.121	2.123	2.104	2.110	2.101	2.098	2.110	2.260	2.047	2.017	2.005	2.232	2.014	2.096
GPAW QM/MM MD avg.	2.185	2.186	2.193	2.193	2.192	2.194	2.190	2.132	2.139	2.118	2.110	2.105	2.106	2.118
	HS													
Orca, PBE, TZVP vacuum	2.131	2.132	2.111	2.111	2.103	2.102	2.115	2.194	2.192	2.132	2.135	2.119	2.119	2.149
Orca, PBE, TZVP COSMO(acn)	2.110	2.111	2.099	2.099	2.093	2.092	2.101	2.142	2.149	2.124	2.130	2.114	2.114	2.129
GPAW QM/MM MD avg.	2.176	2.173	2.165	2.162	2.159	2.156	2.165	2.211	2.214	2.199	2.199	2.196	2.194	2.202

Table S1 shows the thermally averaged bond lengths, compared to conventional geometry optimizations. For the LS state, the study has been extended to encompass a variety of functionals and basis sets. First, the Generalized Gradient Approximation-style PBE[7] functional also used in the QM/MM MD simulations, together with the Ahlrichs-style TZVP basis.[8] Then, the hybrid functional PBE0, where the total exchange energy is obtained by adding 25% exact exchange energy and 75% PBE exchange.[9] This functional is used in conjunction with the Pople-style double-ζ quality basis set 6-31G(d,p),[10–12] as also done elsewhere.[13] For comparison, optimizations have also been carried out using the Ahlrichs-style triple-ζ basis, def2-TZVP.[14] At last, geometry optimizations are carried using the hybrid B3LYP[15,16] functional (20% exact exchange). The simulations marked with '*' uses the Stuttgart-Dresden effective core potential,[17] to be identical to previously carried out work.[13] The calculations

labeled 'COSMO(acn)' employs a dielectric continuum of acetonitrile parameters using the COSMO model.[18] On average, only the GPAW QM/MM MD results achieve the experimental 0.20 Å HS bond elongation, with the dielectric continuum model undershooting the bond stretch, giving 0.17 Å. For the geometry optimizations in the LS state, bond lengths rounding off to < 2.1 Å are marked blue, and bonds rounding off to ≥ 2.1 Å are marked red, to provide an easier overview. Except for B3LYP, we note a 4/2 distortion of the Co-N bonds with the b and h bonds extending ~ 0.1 Å, and the v bonds virtually unchanged, when using Ahlrics style basis sets, whereas the Pople-style basis sets seem to favour a 2/4 distortion, showing that the results are very sensitive to both size and style of basis set, but also to the chosen combination of functional and basis. This is expected, as the relevant energy levels are almost degenerate, and the orbitals do indeed interchange dynamically, as the QM/MM MD simulations described in the main text reveals.

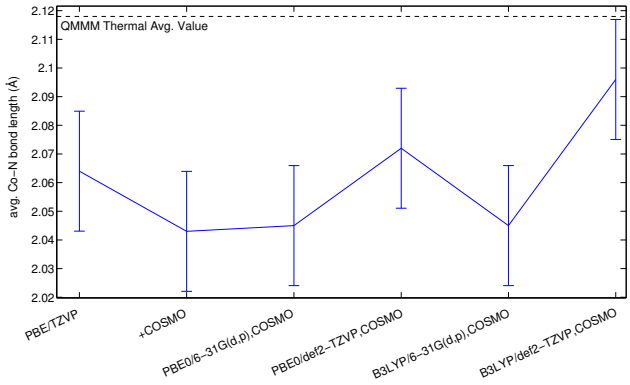

Figure S3: Comparison of the spread of the average Co-N bond results from conventional geometry optimizations with the QM/MM thermal averages. The errorbars represent a 95% confidence interval.

Figure S3 shows that the final thermal Co-N bond length average from the QM/MM simulations do not fall in the a 95% confidence interval of the basis- and functional-induced spread of distances, indicating that the effects of explicit solvation are larger than basis set/functional-induced discrepancies.

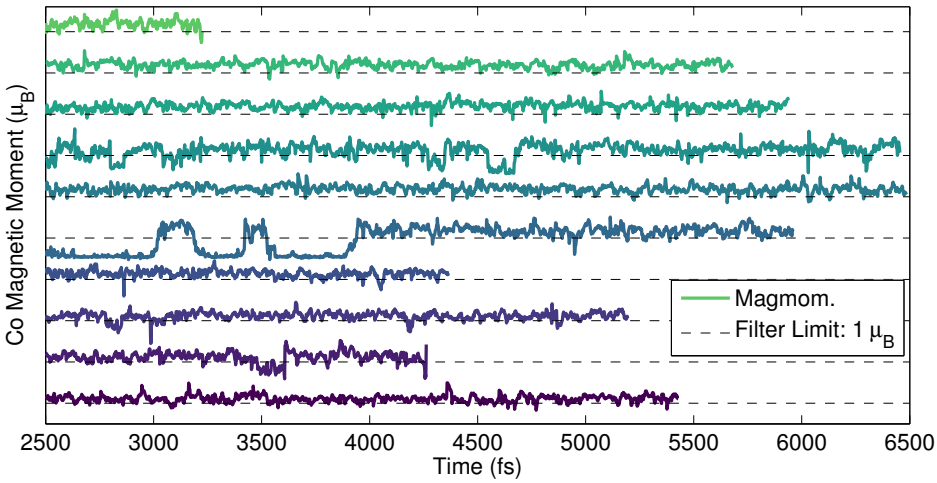

Figure S4: The local Co magnetic moment in units of the Bohr magneton, μ_B, for each individual LS trajectory.

Discerning between $[^3Ru^{II}{=}^1Co^{III}]$ and $[^2Ru^{III}{=}^2Co^{II}]$

In the LS trajectories, the local magnetic moments were read out at each MD step. When the local magnetic moment on the Co centre is > 1 μ_B, it can readily be assumed than the system is in the charge-separated $[^2Ru^{III}{=}^2Co^{II}]$ state. The figure S4 shows how the filter is constructed for the analysis in the main text: Each line shows the sampled magnetic moments of each individual trajectory, and the dashed lines show the applied limit.

Torsions

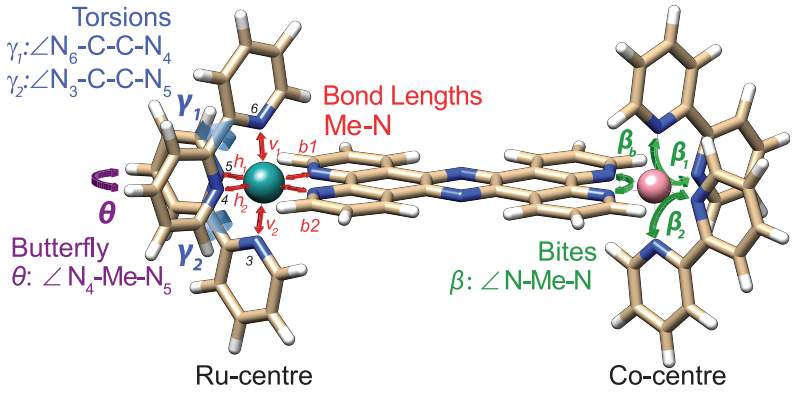

Figure S5: The relevant geometric definitions of [Ru=Co].

Figure S6 shows the dihedral N-C-C-N torsions γ_1 and γ_2 (se figure S5 for definitions).

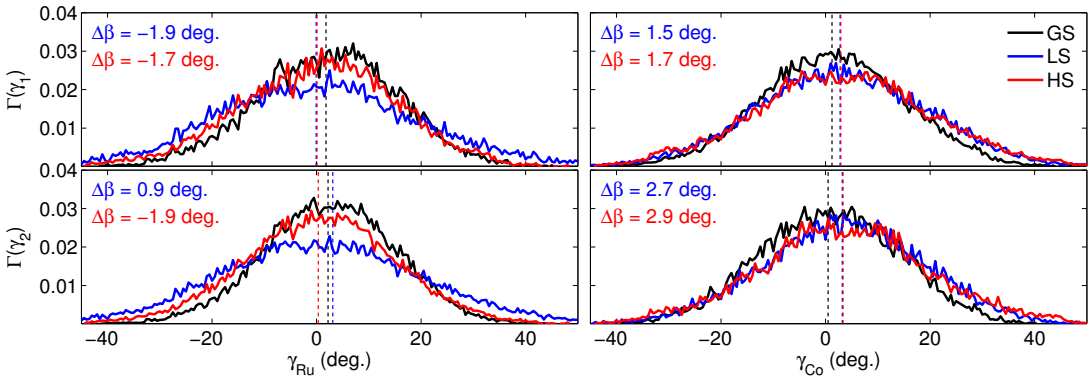

Figure S6: Thermal distributions of torsions.

The Co γ increases on average by $\sim 2^\circ$ in the HS state, while decreasing for the Ru centre.

References

(1) Dohn, A. O.; Jónsson, E. O.; Kjær, K. S.; B. van Driel, T.; Nielsen, M. M.; Jacobsen, K. W.; Henriksen, N. E.; Møller, K. B. Direct Dynamics Studies of a Binuclear Metal Complex in Solution: The Interplay Between Vibrational Relaxation, Coherence, and Solvent Effects. *J. Phys. Chem.. Lett.* **2014**, *5*, 2414–2418.

(2) Dohn, A. O.; Henriksen, N. E.; Møller, K. B. *Transient Changes in Molecular Geometries and How to Model Them*; Springer International Publishing, 2014.

(3) Jónsson, E. Ö.; Thygesen, K. S.; Ulstrup, J.; Jacobsen, K. W. *Computational Approach to Electron Charge Transfer Reactions*; 2014.

(4) Waldman, M.; Hagler, A. New combining rules for rare gas van der waals parameters. *J. Comput. Chem.* **2004**, *14*, 1077.

(5) Mortensen, J.; Hansen, L.; Jacobsen, K. W. Real-space grid implementation of the projector augmented wave method). *Phys. Rev. B* **2005**, *71*, 035109.

(6) Neese, F. ORCA - An ab initio, DFT and semiempirical SCF-MO package - version 2.8. 2010.

(7) Perdew, J. P.; Burke, K.; Ernzerhof, M. Generalized gradient approximation made simple. *Phys. Rev. Lett.* **1996**, *77*, 3865–3868.

(8) Schäfer, A.; Horn, R.; Ahlrichs, R. Fully optimized contracted gaussian basis sets for atoms Li to Kr. *J. Chem. Phys.* **1992**, *97*, 2571–2577.

(9) Adamo, C.; Barone, V. J. Toward reliable density functional methods without adjustable parameters: The PBE0 model. *J. Chem. Phys.* **1999**, *110*, 6158–6170.

(10) Hehre, W.; Ditchfield, R.; Pople, J. Self-Consistent Molecular Orbital Methods. 12. Further extensions of Gaussian-type basis sets for use in molecular-orbital studies of organic-molecules. *J. Chem. Phys.* **1972**, *56*, 2257.

(11) Francl, M. M.; Pietro, W. J.; Hehre, W. J.; Binkley, J. S.; DeFrees, D. J.; Pople, J. A.; Gordon, M. S. Self-Consistent Molecular Orbital Methods. 23. A polarization-type basis set for 2nd-row elements. *J. Chem. Phys.* **1982**, *77*, 3654–3665.

(12) Rassolo, V. A.; Pople, J. A.; Ratner, M. A.; Windus, T. L. 6-31G* basis set for atoms K through Zn. *J. Chem. Phys.* **1998**, *109*, 1223–1229.

(13) Kuhar, K.; Fredin, A.; Persson, P. Exploring Photoinduced Excited State Evolution in Heterobimetallic Ru(II)-Co(III) Complexes. *J. Phys. Chem. B* **2015**, *119*, 7378–7392.

(14) Weigend, F.; Ahlrichs, R. Balanced basis sets of split valence, triple zeta valence and quadruple zeta valence quality for H to Rn: Design and assessment of accuracy. *Phys. Chem. Chem. Phys.* **2005**, *7*, 3297–3305.

(15) Becke, A. D. Density-Functional Thermochemistry. III. The Role of Exact Exchange. *J. Chem. Phys.* **1993**, *98*, 5648–5652.

(16) Stephens, P. J.; Devlin, F. J.; Chabalowski, C. F.; Frisch, M. J. Ab-Initio Calculation of Vibrational Absorption and Circular-Dichroism Spectra Using Density-Functional Force-Fields. *J. Phys. Chem.* **1994**, *98*, 11623–11627.

(17) Dolg, M.; Wedig, U.; Stoll, H.; Preuss, H. Energy-Adjusted Ab Initio Pseudopotentials for the First Row Transition Elements. *J. Chem. Phys.* **1987**, *86*, 866.

(18) Sinnecker, S.; Rajendran, A.; Klamt, A.; Diedenhofen, M.; Neese, F. Calculation of Solvent Shifts on Electronic G-Tensors with the Conductor-Like Screening Model (COSMO) and its Self-Consistent Generalization to Real Solvents (COSMO-RS). *J. Phys. Chem. A* **2006**, *110*, 2235–2245.